Green's functions for transversely isotropic piezoelectric multilayered half-spaces

E. PAN and F. HAN

Department of Civil Engineering, The University of Akron, Akron, OH 44325-3905 U.S.A.
E-mail: pan2@uakron.edu

Abstract. This paper presents Green's functions for transversely isotropic piezoelectric and layered half-spaces. The surface of the half-space can be under general boundary conditions and a point source (point-force/point-charge) can be applied to the layered structure at any location. The Green's functions are obtained in terms of two systems of vector functions, combined with the propagator-matrix method. The most noticeable feature is that the homogeneous solution and propagator matrix are independent of the choice of the system of vector functions, and can therefore be treated in a unified manner. Since the physical-domain Green's functions involve improper integrals of Bessel functions, an adaptive Gauss-quadrature approach is applied to accelerate the convergence of the numerical integral. Typical numerical examples are presented for four different half-space models, and for both the spring-like and general traction-free boundary conditions. While the four half-space models are used to illustrate the effect of material stacking sequence and anisotropy, the spring-like boundary condition is chosen to show the effect of the spring constant on the Green's function solutions. In particular, it is observed that, when the spring constant is relatively large, the response curve can be completely different to that when it is small or when it is equal to zero, with the latter corresponding to the traction-free boundary condition.

Key words: multilayered structure, piezoelectric Green's function, propagator-matrix method, spring-like boundary condition, transverse isotropy

1. Introduction

It is well known that Green's function (*i.e.*, the fundamental solutions due to a concentrated source) is of great importance in the areas of theoretical and applied mathematics and mechanics [1, Chapters 3 and 5; 2, Chapter 6]. While most two-dimensional (2D) elastic Green's functions can be found in the book by Ting [3, Chapter 8], a brief review on the three-dimensional (3D) Green's functions in anisotropic half-spaces can be found in a recent paper by Pan [4] where the author also derived the Green's functions in the anisotropic half-space under general surface boundary conditions.

Although the static Green's function for purely elastic and layered solids has been extensively studied [5–10], relatively little can be found in the literature for the corresponding piezoelectric solids. The available piezoelectric Green's functions include those for a half-space and bimaterials of transversely isotropic piezoelectric material [11–13] and those for general anisotropic piezoelectric infinite spaces [14], anisotropic piezoelectric half-spaces under general boundary conditions [15], and the corresponding bimaterials [16, 17]. A brief review on the 3D piezoelectric Green's functions can also be found in Pan [18].

In the study of multilayered systems, it is found that the two systems of vector functions introduced previously by Pan [19, 20] in combination with the propagator-matrix method [5, 21] are very convenient. The systems of vector functions possess certain advantages as
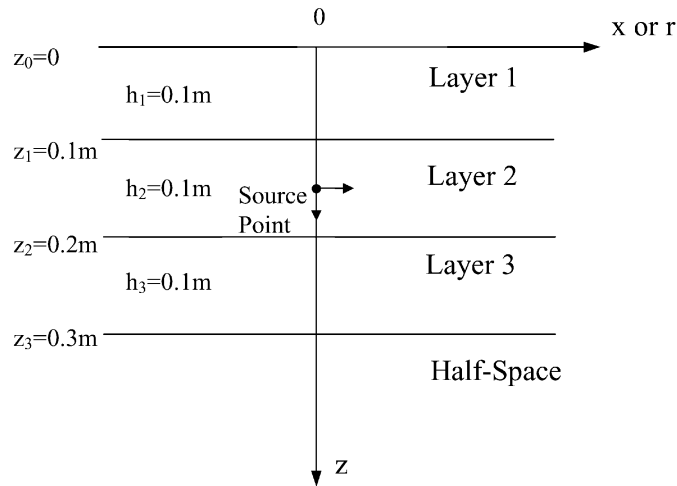
Figure with labels:

z₀=0, h₁=0.1m, Layer 1, 0, x or r
z₁=0.1m, h₂=0.1m, Source Point, Layer 2
z₂=0.2m, h₃=0.1m, Layer 3
z₃=0.3m, Half-Space
z

Figure 1. Geometry of a three-layered piezoelectric half-space.

compared to the Fourier or Hankel transform. For example, the vector-function systems can express any integrable vector-function, while the Fourier and Hankel transforms can do so for scalar functions only. Another advantage is that, for elastic problems with relatively higher material symmetry, the propagator matrices in these two vector systems are exactly the same and the problems of axially symmetric and 2D deformations can all be included as special cases of the general solutions [19, 20]. This approach has been extended and applied by Ding and Shen [22] and Huang [23] to some geophysical problems, and recently by Pan [24] and Pan and Heyliger [25] to the static and vibration problems of multilayered magneto-electro-elastic rectangular plates with simply supported edges.

In this paper, we further apply the system of vector functions and the propagator-matrix method to derive the Green's functions in multilayered and transversely isotropic piezoelectric half-spaces. The boundary condition on the surface of the layered half-space can be the general spring-like ones, which include the previously studied surface conditions as special cases. In the transformed domain, we proposed a solution method in which the propagator matrices can be multiplied directly without any overflow; thus, the matrix propagation can be performed very efficiently. The physical-domain Green's functions are then obtained employing an adaptive Gauss quadrature [26, 27]. Numerical examples are presented for four layered half-space models made of the poled lead-zirconate-titanate (PZT-4) ceramic and $BaTiO_3$, which illustrate clearly the effect of material stacking sequence and anisotropy. Also investigated in this paper is the influence of the spring constant on the induced fields. It is shown that, when the spring constant is relatively large, the response curve can be completely different to that when it is small. While the numerical results may have potential applications in different areas where layered structures are involved, the methodology could be extended to problems involving other concentrated sources, such as eigenstrain and dislocation.

2. Governing equations and systems of vector functions

Let us consider a piezoelectric structure made up of $p-1$ parallel, homogeneous, transversely isotropic, and piezoelectric layers lying over a homogeneous, transversely isotropic, and piezoelectric half-space. The layers are numbered serially with the layer at the top being

layer 1 and the half-space being layer p (see Figure 1 for a four-layered system). We place the Cartesian and/or cylindrical coordinates at the surface, and the z-axis is drawn downwards into the layered half-space. The j-th layer is bounded by the interfaces $z = z_{j-1}, z_j$. It is obvious that $z_0 = 0$ and $z_{p-1} = H$, where H is the depth of the last interface. In the derivation given below, we choose the Cartesian system of vector functions, the results in the corresponding cylindrical system of vector functions for the piezoelectric case can be extended from previous purely elastic solutions [5, 19, 20].

For a transversely isotropic and piezoelectric linear solid, we have the following governing equations:

1). Equilibrium equations

$$\sigma_{ij,j} + f_i = 0, \tag{1}$$

$$D_{i,i} - q = 0, \tag{2}$$

where σ_{ij} and D_i are the stress and electric displacement, respectively; f_i and q are the body force and electric-charge density, which will be replaced later by a concentrated force and electric charge. In this paper, summation over repeated lowercase (uppercase) subscripts is implied. A subscript comma denotes partial differentiation with respect to the coordinates (*i.e.*, x, y, z);

2). Constitutive relations

$$\begin{aligned}
\sigma_{xx} &= C_{11}\gamma_{xx} + C_{12}\gamma_{yy} + C_{13}\gamma_{zz} - e_{31}E_z, \\
\sigma_{yy} &= C_{12}\gamma_{xx} + C_{11}\gamma_{yy} + C_{13}\gamma_{zz} - e_{31}E_z, \\
\sigma_{zz} &= C_{13}\gamma_{xx} + C_{13}\gamma_{yy} + C_{33}\gamma_{zz} - e_{33}E_z, \\
\sigma_{yz} &= 2C_{44}\gamma_{yz} - e_{15}E_y, \\
\sigma_{xz} &= 2C_{44}\gamma_{xz} - e_{15}E_x, \\
\sigma_{xy} &= 2C_{66}\gamma_{xy},
\end{aligned} \tag{3}$$

$$\begin{aligned}
D_x &= 2e_{15}\gamma_{xz} + \varepsilon_{11}E_x, \\
D_y &= 2e_{15}\gamma_{yz} + \varepsilon_{11}E_y, \\
D_z &= e_{31}(\gamma_{xx} + \gamma_{yy}) + e_{33}\gamma_{zz} + \varepsilon_{33}E_z,
\end{aligned} \tag{4}$$

where γ_{ij} is the elastic strain and E_i electric field; C_{ij}, e_{ij}, and ε_{ij} are the elastic moduli, piezoelectric coefficients, and dielectric constants, respectively;

3). Elastic displacement-strain and electric potential-electric field relations

$$\gamma_{ij} = 0.5(u_{i,j} + u_{j,i}),$$

$$E_i = -\phi_{,i},$$

where u_i and ϕ are the elastic displacement and electric potential, respectively.

We now introduce the following Cartesian system of vector functions [19, 20]:

$$\begin{aligned}
\boldsymbol{L}(x, y; \alpha, \beta) &= \boldsymbol{e}_z S(x, y; \alpha, \beta), \\
\boldsymbol{M}(x, y; \alpha, \beta) &= (\boldsymbol{e}_x \partial_x + \boldsymbol{e}_y \partial_y) S(x, y; \alpha, \beta), \\
\boldsymbol{N}(x, y; \alpha, \beta) &= (\boldsymbol{e}_x \partial_y - \boldsymbol{e}_y \partial_x) S(x, y; \alpha, \beta),
\end{aligned} \tag{5}$$

with

$$S(x, y; \alpha, \beta) = e^{-i(\alpha x + \beta y)}/(2\pi), \tag{6}$$

where e_x, e_y, and e_z are the unit vectors along the x-, y-, and z-axes, respectively; α and β are the transformation variables to the two horizontal physical variables x and y. There are two important features associated with this system of vector functions: (1) for plane-strain deformation in the (x, z)-plane, one needs only to replace 2π by $\sqrt{2\pi}$ and β by 0, respectively; (2) while the solution in terms of the L & M vectors is contributed to the dilatational deformation, that of the N vector to the rotational part. Corresponding to the dynamic counterparts, the L & M part is related to the Rayleigh wave, whilst the N part to the Love wave. In this paper we name the solution associated with the L & M vectors as LM-type solution and that associated with the N vector as N-type solution.

3. General solution and propagator matrix

We now express the elastic displacement, electric potential, traction, electric displacements, body force, and negative electric-charge density in terms of the Cartesian system of vector functions (*i.e.*, Equation (5)),

$$u(x, y, z) = \int\int_{-\infty}^{+\infty} [U_L(z)L(x, y) + U_M(z)M(x, y) + U_N(z)N(x, y)]d\alpha d\beta, \tag{7}$$

$$\phi(x, y, z) = \int\int_{-\infty}^{+\infty} \Phi(z)S(x, y)d\alpha d\beta, \tag{8}$$

$$t(x, y, z) \equiv \sigma_{xz}e_x + \sigma_{yz}e_y + \sigma_{zz}e_z = \int\int_{-\infty}^{+\infty}[T_L(z)L(x, y) + T_M(z)M(x, y) \\ + T_N(z)N(x, y)]d\alpha d\beta, \tag{9}$$

$$D(x, y, z) = \int\int_{-\infty}^{+\infty} [D_L(z)L(x, y) + D_M(z)M(x, y) + D_N(z)N(x, y)]d\alpha d\beta, \tag{10}$$

$$f(x, y, z) = \int\int_{-\infty}^{+\infty} [F_L(z)L(x, y) + F_M(z)M(x, y) + F_N(z)N(x, y)]d\alpha d\beta, \tag{11}$$

$$-q(x, y, z) = \int\int_{-\infty}^{+\infty} Q(z)S(x, y)d\alpha d\beta. \tag{12}$$

Taking the derivatives of the elastic displacement (7) and electric potential (8), and substituting the results in the constitutive relations (3) and (4), we can also express the elastic stress and electric displacement in terms of the Cartesian system of vector functions. Furthermore, comparing these elastic stress and electric displacement with (9) and (10), we found

$$T_L = -\lambda^2 C_{13}U_M + C_{33}\frac{dU_L}{dz} + e_{33}\frac{d\Phi}{dz},$$

$$T_M = C_{44}(U_L + \frac{dU_M}{dz}) + e_{15}\Phi, \tag{13a,b,c}$$

$$T_N = C_{44}\frac{dU_N}{dz},$$

$$D_L = -\lambda^2 e_{31}U_M + e_{33}\frac{dU_L}{dz} - \varepsilon_{33}\frac{d\Phi}{dz}. \tag{14}$$

By substituting the elastic stress and electric displacement in (1) and (2), with the body force f and electric charge density q being replaced by (11) and (12), we obtained

$$\frac{dT_L}{dz} - \lambda^2 T_M + F_L = 0,$$
$$-\lambda^2 C_{11} U_M + C_{13}\frac{dU_L}{dz} + \frac{dT_M}{dz} + e_{31}\frac{d\Phi}{dz} + F_M = 0, \qquad (15a,b,c)$$
$$\frac{dT_N}{dz} - \lambda^2 C_{66} U_N + F_N = 0,$$

$$\frac{dD_L}{dz} - \lambda^2 e_{15}(\frac{dU_M}{dz} + U_L) + \lambda^2\varepsilon_{11}\Phi + Q = 0, \qquad (16)$$

where

$$\lambda = \sqrt{\alpha^2 + \beta^2}.$$

3.1. N-TYPE SOLUTION

It is observed from (13) to (16) that the *N*-type solution is independent of the rest. This is one of the advantages of using the system of vector functions. Furthermore, the *N*-type is independent of the electric quantities, *i.e.*, it is purely elastic. Therefore, previous results for the purely elastic case can be directly borrowed [19]. In other words, the general solution can be expressed as [19]

$$[E^N] = [Z^N(z)][K^N], \qquad (17)$$

where $[K^N]$ is a column coefficient vector of 2×1 with its elements to be determined by the continuity and/or boundary conditions. Also in (17),

$$[E^N(z)] = [U_N(z), T_N(z)/\lambda]^t \qquad (18)$$

and $[Z^N(z)]$ is the solution matrix given in [19].

The propagating relation that relates the expansion coefficients U_N and T_N at the upper interface to the lower interface of layer *j* can be found as

$$\left[E^N(z_{j-1})\right] = [a^N]\left[E^N(z_j)\right], \qquad (19)$$

where z_{j-1} and z_j are the depths of the top and bottom interfaces of layer *j*, and $[a^N]$ is the so-called propagator matrix (or layer matrix, or transfer matrix) given in [19].

We remark that the solution and propagator matrices in the cylindrical system of vector functions are exactly the same as that in the Cartesian system, respectively. This feature gives certain numerical advantages when programming these equations in the two systems of vector functions.

3.2. LM-TYPE SOLUTION

For this type of deformation, the elastic and piezoelectric fields are coupled. In order to solve the coupled problem, we first derive, from (13) to (16), the following compact form of equations for the *LM*-type:

$$[U_L, U_M, T_L, T_M, \Phi, D_L]^t_{,z} = [A][U_L, U_M, T_L, T_M, \Phi, D_L] + [0, 0, -F_L, -F_M, 0, -Q]^t, \qquad (20)$$

where the nonzero elements of the 6×6 matrix $[A]$ are given in Appendix A. It is remarked that the diagonal elements of $[A]$ are zero, a feature that will be used soon. We now introduce the column vector

$$[E] = [U_L, \lambda U_M, T_L/\lambda, T_M, \Phi, D_L/\lambda]^t,$$

so that (20) becomes

$$[E]_{,z} = \lambda[W][E] + [F], \tag{21}$$

where the force expansion column vector is

$$[F] = [0, 0, -F_L/\lambda, -F_M, 0, -Q/\lambda]^t.$$

The nonzero elements of the 6×6 matrix $[W]$ in (21) are given in Appendix B.

To find the homogeneous solution of (21), we assume that

$$[E(z)] = [b]e^{\lambda \eta z}. \tag{22}$$

Substituting (22) in (21) and noticing that all the diagonal elements of $[W]$ are zero, we obtain the following 6-dimensional eigenequations for the corresponding homogeneous part of (21)

$$\{[W] - \eta[I]\}[b] = 0, \tag{23}$$

where $[I]$ is the 6×6 identity matrix.

It is observed from (23) that the eigenvalues and their corresponding eigenvectors are independent of the integral variable λ! Therefore, these eigenequations need to be solved only once for each layer for the given material properties.

Let us, therefore, assume that the 6 eigenvalues are distinct; the general solution corresponding to the homogeneous part of (21) is then obtained as

$$[E(z)] = [Z(z)][K], \tag{24}$$

where $[K]$ is a 6×1 coefficient matrix with its elements to be determined by the interface and/or boundary conditions, and

$$[Z(z)] = [B]\left\langle e^{\lambda \eta^* z} \right\rangle \tag{25}$$

with

$$\left\langle e^{\lambda \eta^* z} \right\rangle = \mathrm{diag}[e^{\lambda \eta_1 z}, e^{\lambda \eta_2 z}, e^{\lambda \eta_3 z}, e^{-\lambda \eta_1 z}, e^{-\lambda \eta_2 z}, e^{-\lambda \eta_3 z}]$$

$$[B] = [b_1, b_2, b_3, b_4, b_5, b_6].$$

It is noted that, while the first 3 eigenvectors correspond to the first 3 eigenvalues with positive real parts, the last 3 eigenvectors correspond to the last 3 eigenvalues, which have opposite signs to the first 3 eigenvalues.

From (24), we obtain the propagating relation

$$[E(z_{j-1})] = [a][E(z_j)], \tag{26}$$

where,

$$[\boldsymbol{a}] = [\boldsymbol{B}]\left\langle e^{-\lambda \eta^* h_j}\right\rangle[\boldsymbol{B}]^{-1} \tag{27}$$

is the propagator matrix for the *LM*-type deformation.

Again, similar to the *N*-type solution, the solution and propagator matrices in the cylindrical system of vector functions are exactly the same as (25) and (27), respectively. This feature can be utilized in programming these equations in the two systems of vector functions.

It is also noted that in solving the eigenequation (23), we have assumed that all the eigenvalues are distinct. Should repeated eigenvalues occur, a slight perturbation on the material properties could be used to make the eigenvalues distinct with neglected errors, so that the solution developed in this paper is still valid.

4. General boundary condition and source function

Following Ting [3] and Pan [4, 15], we write the general boundary condition on the surface of the multilayered half-space in the following matrix form

$$[\boldsymbol{k}^u][\boldsymbol{u}] + [\boldsymbol{k}^t][\boldsymbol{t}] = [\boldsymbol{0}], \tag{28}$$

where the vector $[\boldsymbol{u}]=\{u_x, u_y, u_z, \phi\}^t$ consists of the elastic displacement and electric potential, and $[\boldsymbol{t}]=\{\sigma_{xz}, \sigma_{yz}, \sigma_{zz}, D_z\}^t$ consists of the traction and the normal electric displacement component. The $4{\times}4$ matrices $[\boldsymbol{k}^u]$ and $[\boldsymbol{k}^t]$ define the general spring-like relation between the vectors $[\boldsymbol{u}]$ and $[\boldsymbol{t}]$ on the surface of the layered half-space, which includes the homogeneous boundary condition studied in Ting [3] and Pan [4, 15] as a special case. Furthermore, the right-hand side of (28) can be nonzero, thus containing the general surface load condition if necessary.

For given matrices $[\boldsymbol{k}^u]$ and $[\boldsymbol{k}^t]$ in (28), we can in general connect the coefficients $[\boldsymbol{E}^N]$ in (17) and $[\boldsymbol{E}]$ in (21) to the coefficients of the boundary vectors $[\boldsymbol{u}]$ and $[\boldsymbol{t}]$. By use of the propagator matrix method, the given problem can then be solved for the layered system. For the special cases discussed in Ting [3] and Pan [4, 15], the displacement and traction is uncoupled on the surface and the resulting boundary condition for the coefficients $[\boldsymbol{E}^N]$ and $[\boldsymbol{E}]$ is trivial, as will become clear soon. However, the present method can handle the general boundary condition described by (28). As an example, we will study the following spring-like case, where $[\boldsymbol{k}^t]$ is a 4×4 identity matrix. In other words, (28) is reduced to

$$[\boldsymbol{k}^u][\boldsymbol{u}] + [\boldsymbol{t}] = [\boldsymbol{0}]. \tag{29}$$

To solve the boundary-value problem, we also need to specify the point source to the layered system. We assume, without loss of generality, that there is a point-force/negative point-charge located along the *z*-axis at the depth $z = h$ (see Figure 1 for example), *i.e.*,

$$f_i(x, y, z) = \delta(x)\delta(y)\delta(z - h)n_i, \tag{30}$$

$$-q(x, y, z) = \delta(x)\delta(y)\delta(z - h). \tag{31}$$

Expanding (30) and (31), and making use of (11) and (12), we found the expansion coefficients as [28].

$$F_L = \frac{n_z}{2\pi}\delta(z - h), \quad F_M = \frac{n_x\alpha + n_y\beta}{2\pi\lambda^2}\delta(z - h), \tag{32}$$

$$F_N = \frac{n_x\beta - n_y\alpha}{2\pi\lambda^2}\delta(z - h), \quad Q = \frac{-1}{2\pi}\delta(z - h). \tag{33}$$

We remark again that the coefficients for the corresponding 2D (x,z)-plane strain deformation can be obtained from (32) and (33) by replacing 2π by $\sqrt{2\pi}$ and β by 0.

The concentrated force and electric charge will induce discontinuities in the expansion coefficients of the traction and normal electric displacement component. These are found to be

$$\Delta T_L \equiv T_L(h + 0) - T_L(h - 0) = \frac{-n_z}{2\pi},$$
$$\Delta T_M \equiv T_M(h + 0) - T_M(h - 0) = -\frac{n_x\alpha + n_y\beta}{2\pi\lambda^2}, \tag{34}$$

$$\Delta T_N \equiv T_N(h + 0) - T_N(h - 0) = -\frac{n_x\beta - n_y\alpha}{2\pi\lambda^2},$$
$$\Delta D_L \equiv D_L(h + 0) - D_L(h - 0) = \frac{1}{2\pi}. \tag{35}$$

5. Solution for multilayers

Let a source be situated at depth $z = h$ in layer s. We divide the source layer into two sub-layers, $s1$ and $s2$, with identical properties. Because of the presence of the source, some components of functions $[E(z)]$ and $[E^N(z)]$ will be discontinuous across $z = h$. In general, the discontinuities can be defined as

$$[\Delta E] \equiv [E_{s2}(h)] - [E_{s1}(h)],$$
$$[\Delta E^N] \equiv [E_{s2}^N(h)] - [E_{s1}^N(h)]$$

with their discontinuity components being given by (34) and (35).

Propagating the solution from the top of the source $z = h - 0$ to the surface $z = 0$, we have

$$[E(0)] = [a_1][a_2] - - - [a_{s1}][E_{s1}(h)],$$
$$[E^N(0)] = [a_1^N][a_2^N] - - - [a_{s1}^N][E_{s1}^N(h)] \tag{36a,b}$$

Similarly, propagating the solutions from the half-space $z = H$ to the bottom of the source $z = h + 0$, we obtain

$$[E_{s2}(h)] = [a_{s2}][a_{s+1}] - - - [a_{p-1}][Z_p(H)][K_p],$$
$$[E_{s2}^N(h)] = [a_{s2}^N][a_{s+1}^N] - - - [a_{p-1}^N][Z_p^N(H)][K_p^N] \tag{37a,b}$$

with the undetermined coefficients having the structure

$$[K_p] = [0, 0, 0, *, *, *]^t,$$
$$[K_p^N] = [0, *]^t \tag{38a,b}$$

to satisfy the requirement that the solution vanishes when z approaches $+\infty$. In (38), the symbol '*' denotes an unknown coefficient.

From (36) and (37), we find

$$[E(0)] = [G][K_p] - [R],$$
$$[E^N(0)] = [G^N][K_p^N] - [R^N],$$

(39a,b)

where

$$[G] = [a_1][a_2] - - - [a_{p-1}][Z_p(H)],$$
$$[G^N] = [a_1^N][a_2^N] - - - [a_{p-1}^N][Z_p^N(H)],$$
$$[R] = [a_1][a_2] - - - [a_{s-1}][a_{s1}][\Delta E],$$
$$[R^N] = [a_1^N][a_2^N] - - - [a_{s-1}^N][a_{s1}^N][\Delta E^N].$$

(40a,b)

Using the boundary condition at $z = 0$, the unknown coefficients in $[K_p]$ and $[K_p^N]$ can be determined. For example, for the traction-free insulating and traction-free conducting boundary conditions at the surface, we have, respectively

$$T_L(0) = T_M(0) = T_N(0) = D_L(0) = 0,$$
$$T_L(0) = T_M(0) = T_N(0) = \Phi(0) = 0.$$

(41a,b)

That is, we have four conditions to determine four unknowns in $[K_p]$ and $[K_p^N]$. After the unknown coefficients in $[K_p]$ and $[K_p^N]$ are determined, the expansion coefficients at any depth (*e.g.*, for $z \geq h$ in layer j, *i.e.*, $z_{j-1} \leq z \leq z_j$) can be derived exactly as:

$$[E(z)] = [a_{s2}(z - z_{j-1})][a_{s+1}] - - - [a_{p-1}][Z_p(H)][K_p],$$
$$[E^N(z)] = [a_{s2}^N(z - z_{j-1})][a_{s+1}^N] - - - [a_{p-1}^N][Z_p^N(H)][K_p^N].$$

(42a,b)

As discussed in Pan [5], overflow may occur from the multiplication of matrices in (40). This can be overcome by factoring out the exponentially growing factor in the elements of the propagator matrix. Since in the modified propagator matrices, no element is exponentially growing, there will be no overflow problem for a multilayered half-space having any number of layers.

6. Numerical results

The Green's functions obtained above in the transformed domain need to be integrated numerically to find the physical-domain solutions. Since we have expressed the solutions in terms of the cylindrical system of vector functions, the individual components of the Green's functions will be in the cylindrical coordinates. We found that, in order to find all the elastic and electric quantities (elastic displacements, strains, and stresses; electric potential, electric fields, and electric displacements) due to the three point forces and negative point charge density, only 38 integrals need to be evaluated.

It is noted that the integrands in the improper integrals for the Green's functions involve the Bessel function that is oscillatory and goes to zero slowly when its variable approaches infinity. Thus, the common numerical integration methods, such as the trapezoidal rule or Simpson's rule, are not suitable for the current integration. In this paper, an adaptive Gauss quadrature [26, 27] for the numerical integration of Hankel transform is adopted and modified for the evaluation of the Green's functions in multilayered half-spaces.

We first express the improper integral for each Green's function as a summation of partial integration terms:

$$\int\limits_{0}^{+\infty} f(\lambda, z) J_m(\lambda r) \mathrm{d}\lambda = \sum_{n=1}^{N} \int\limits_{\lambda_n}^{\lambda_{n+1}} f(\lambda, z) J_m(\lambda r) \mathrm{d}\lambda. \tag{43}$$

In each subinterval, a starting 3-point Gauss rule is applied to approximate the integral. A combined relative-absolute error criterion is used to check the results. If the error criterion is not satisfied, new Gauss points are added optimally so that only the new integrand values need to be calculated. This procedure continues until the selected error criterion is satisfied. In the numerical analysis presented below, we have set the relative and absolute errors, respectively, at 10^{-3} and 10^{-4}.

The original FORTRAN program was written for one Hankel transform. In our case, evaluation of 38 integrals is required in order to obtain all the elastic and electric components. Thus, direct application of the original adaptive Gauss quadrature would result in intensive computational time because of the multiplication of the propagator matrices involved. However, we noticed that the integrand $f(\lambda,z)$ in (43), which represents one of the expansion coefficients in (42), is actually the result of the multiplication of the propagator matrices. Since for a given layered half-space, the propagator matrix depends only upon the integral variable λ, the original program can therefore be modified in such a way that for all the elastic and electric components, the multiplication of the propagator matrices needs to be evaluated only once for a given Gauss quadrature point λ. It is apparent that such a modification to the original adaptive Gauss quadrature saves substantial computational time when calculating all the Green's components.

We first applied our multilayered Green's function solutions to the pure elastic layered system (with zero piezoelectric coefficients) and homogeneous piezoelectric half-space case (with the same material properties in all the layers). We found that the results from the present multilayered Green's function program are exactly the same as the existing solutions [5, 15].

In our numerical studies, the layered half-space is made of two typical transversely isotropic piezoelectric materials: One is the poled lead-zirconate-titanate (PZT-4) ceramic, the other is $BaTiO_3$ [24], with their properties being given in Appendix C.

In order to study the influence of material stacking sequence as well as layering on the response of the layered half space to the point-force and point-charge, four different layered models are studied (Table 1). It is noted that each layer has the same thickness of $0 \cdot 1$ m while the fourth layer is half-space. It is also obvious that Models I and II are for homogeneous half-spaces.

For all the numerical examples studied in this paper, the source point is located on the z-axis in the middle of the second layer with coordinate (0·0, 0·0, 0·15 m) (Figure 1). The point force has a magnitude of 1N and a negative point charge of magnitude 1C. Also in the paper, all numerical results are presented in dimensionless terms. Thus, the coordinate can be transformed into a dimensional one by simply multiplying L (= 1 m). In order to obtain the dimensional elastic displacement, electric potential, stress, and electric displacement (*i.e.* for stress in N/m^2 and electric displacement in C/m^2), one needs to carry out the following simple multiplication or division (with $C_{max} = 1 \cdot 66 \times 10^{11}$ N/m^2 and $e_{max} = 18 \cdot 6$ C/m^2):

(i)   for the elastic displacement due to a point force, divide the result by $C_{max} L$;

(ii) for the elastic displacement due to a point charge or the electric potential due to a point force, divide the result by $e_{max} L$;

Table 1. Layer number, thickness, and material for the four models.

Layer	Thickness	Material model			
		Model I	Model II	Model III	Model IV
1	0·1 m	PZT-4	BaTiO$_3$	PZT-4	BaTiO$_3$
2	0·1 m	PZT-4	BaTiO$_3$	BaTiO$_3$	PZT-4
3	0·1 m	PZT-4	BaTiO$_3$	PZT-4	BaTiO$_3$
4	Half space	PZT-4	BaTiO$_3$	PZT-4	BaTiO$_3$

(iii) for the electric potential due to a point charge, multiply the result by $C_{max}/(e_{max}^2 L)$;

(iv) for the stress due to a point force or the electric displacement due to a point charge, divide the result by L^2;

(v) for the stress due to a point charge, multiply the result by $C_{max}/(e_{max} L^2)$;

(vi) for the electric displacement due to a point force, multiply the result by $e_{max}/(C_{max} L^2)$;

Two surface boundary conditions are studied: one is the homogeneous traction-free and insulating boundary condition, and the other is the spring-like boundary condition. For the spring-like condition, we choose the coefficient matrix $[k^u]$ in (29) as

$$[k^u] = \text{diag}(0, 0, k_{33}^u, 0),$$

which gives the boundary condition at $z = 0$ as

$$\sigma_{xz} = \sigma_{yz} = D_z = 0, \quad k_{33}^u u_z + \sigma_{zz} = 0.$$

It is apparent that $k_{33}^u \equiv k$ is in the unit of N/m^3 [29]. It is further noticed that this spring constant k is normalized by L/C_{max} in the numerical calculation.

6.1. TRACTION-FREE AND INSULATING SURFACE BOUNDARY CONDITION

6.1.1. *Surface response*

Figures 2a to 2c show the surface variation of u_x, ϕ, and D_x when a negative point charge is applied. While the electric potential follows the same order in magnitudes for the four different models, *i.e.*, I>III>IV>II, the response is also clearly separated into two groups: One group consists of Model I (*i.e.*, homogeneous PZT-4) and Model III (*i.e.*, the layered P/B/P) and the other consists of Model II (*i.e.*, homogeneous BaTiO$_3$) and Model IV (*i.e.*, the layered B/P/B). As for u_x and D_x, one can clearly observe that when x is small (*i.e.*, the near-field), the responses of u_x for Models II and III, and Models I and IV, are, respectively, close to each other (Figure 2a); On the other hand, the responses of D_x for Models I and III, and Models II and IV, are also, respectively, close to each other (Figure 2c).

6.1.2. *Interior response*

For the interior responses studied in this paper, the field points are located on a vertical line varying from (0·1 m, 0·0, 0·0) to (0·1 m, 0·0, 0·3 m). The elastic displacement u_z, stress σ_{xx}, electric potential ϕ, and electric displacement D_x are plotted in Figures 3 and 4 for two different point sources, namely a point force in the x-direction and a point force in the z-direction.
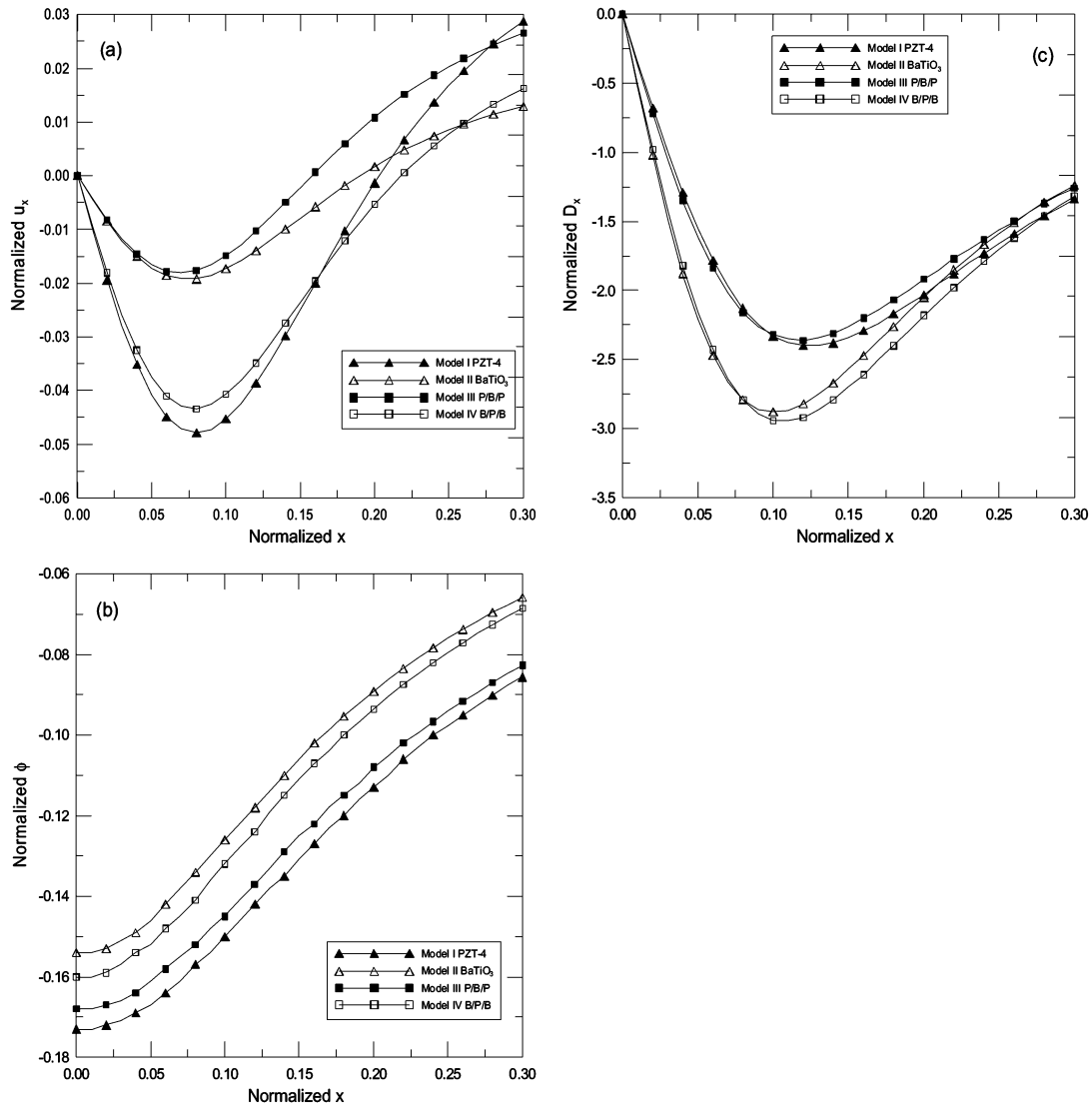
Figure 2. (a)–(c). Variations of field quantities along the surface line (from (0,0,0) to (0·3m,0,0)) of the four half-space models, due to a negative point charge at (0, 0, 0·15m). Displacement component u_x in (a), electric potential ϕ in (b), and electric displacement D_x in (c).

First of all, we observe that, due to material-property discontinuity, stress σ_{xx} and electric displacement D_x show clear discontinuity across the two interfaces at $z = 0·1$ m and $0·2$ m in Model III (P/B/P) and IV (B/P/B) (Figures 3b, 3d, 4b, 4d).

It is also interesting that under the point force in x-direction, the slopes of u_z and D_x are discontinuous across the source point for Models II and III (*i.e.*, when the source is in the BaTiO$_3$ material, Figures 3a and 3d), whilst the same feature is observed for the slope of ϕ for Models I and IV (*i.e.*, when the source is in the PZT-4 material, Figure 3c). Under the
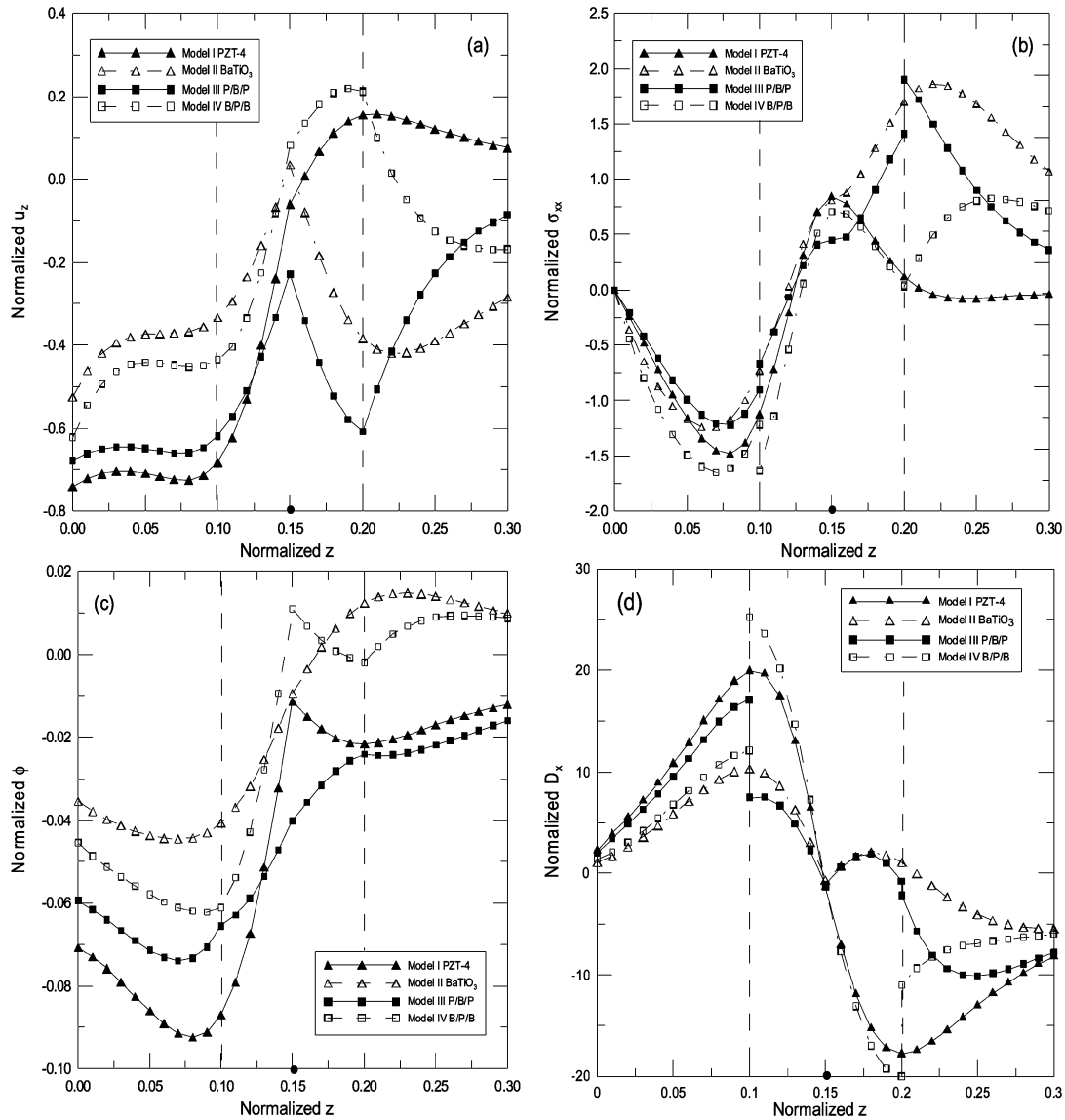
Figure 3. (a)–(d). Variations of field quantities along a vertical line (from (0·1m,0,0) to (0·1m,0,0·3m)) for the four half-space models, due to a point force at (0, 0, 0·15m) in *x*-direction. Displacement component u_z in (a), stress component σ_{xx} in (b), electric potential ϕ in (c), and electric displacement D_x in (d).

point force in the *z*-direction, we also observe that the slope of σ_{xx} is discontinuous across the source point for Models II and III (*i.e.*, when the source is in the BaTiO$_3$ material; Figure 4b).

6.2. SPRING-LIKE SURFACE BOUNDARY CONDITION

Shown in Figures 5a to 5d are the responses of the elastic displacement u_z, stress σ_{xx}, electric potential ϕ, and electric displacement D_x on the surface of Model III half-space (*i.e.*, the P/B/P half space) for different spring constant *k*. The point force is located at (0·0, 0·0, 0·15 m) in the *z*-direction. We first remark that, when *k* is zero, the surface responses are exactly the same
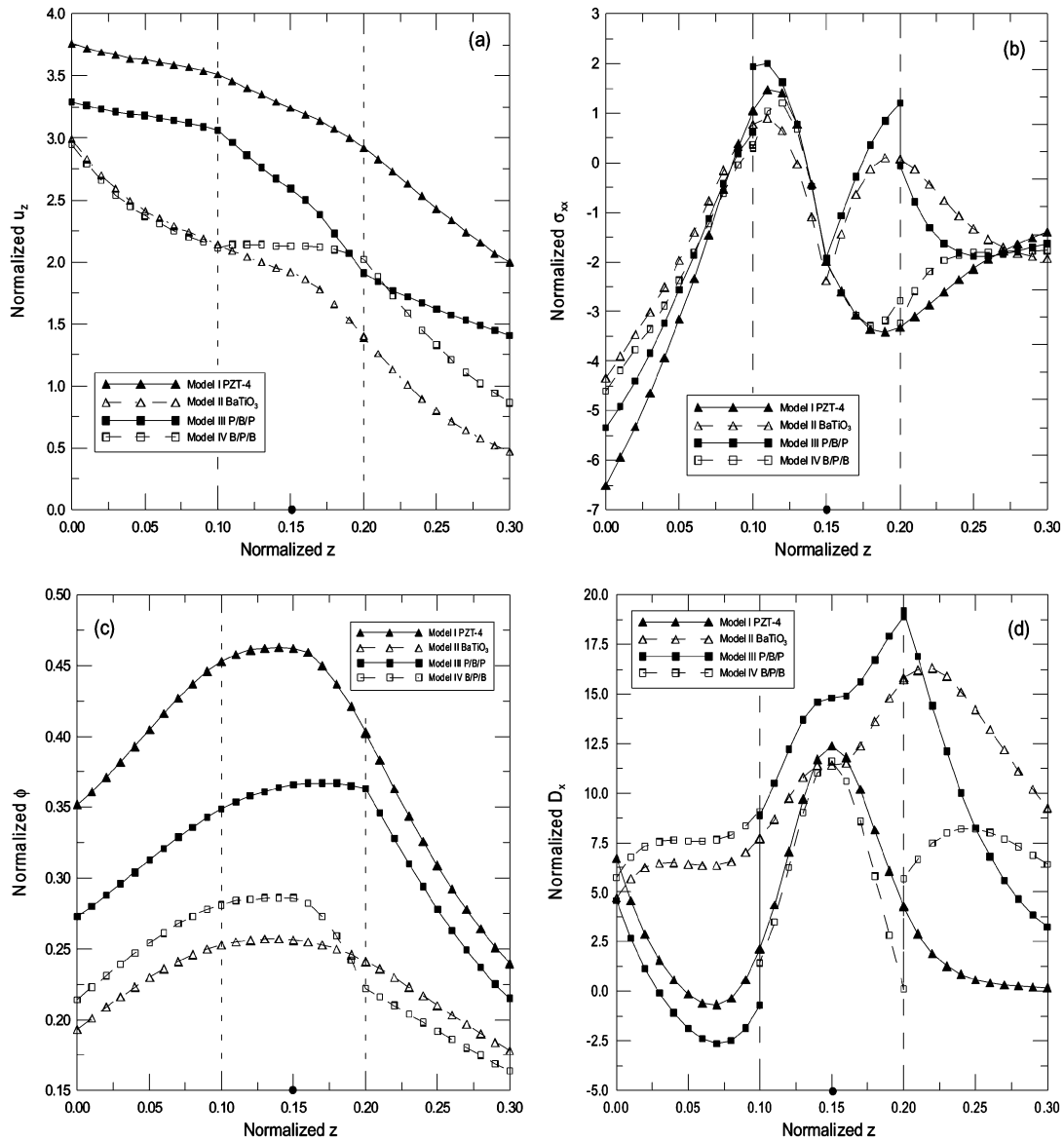
Figure 4. (a)–(d). Variations of field quantities along a vertical line (from (0·1m,0,0) to (0·1m,0,0·3m)) for the four half-space models, due to a point force at (0, 0, 0·15m) in z-direction. Displacement component u_z in (a), stress component σ_{xx} in (b), electric potential ϕ in (c), and electric displacement D_x in (d).

as those based directly on the traction-free and insulating-boundary-condition formulation. When k increases, the effect of the spring-like boundary condition on the field quantities can be clearly observed. This is particularly true when $k \geq 5 \times 10^{11} \mathrm{N/m}^3$, where the curve shapes of the response are completely different to those when k is relatively small.
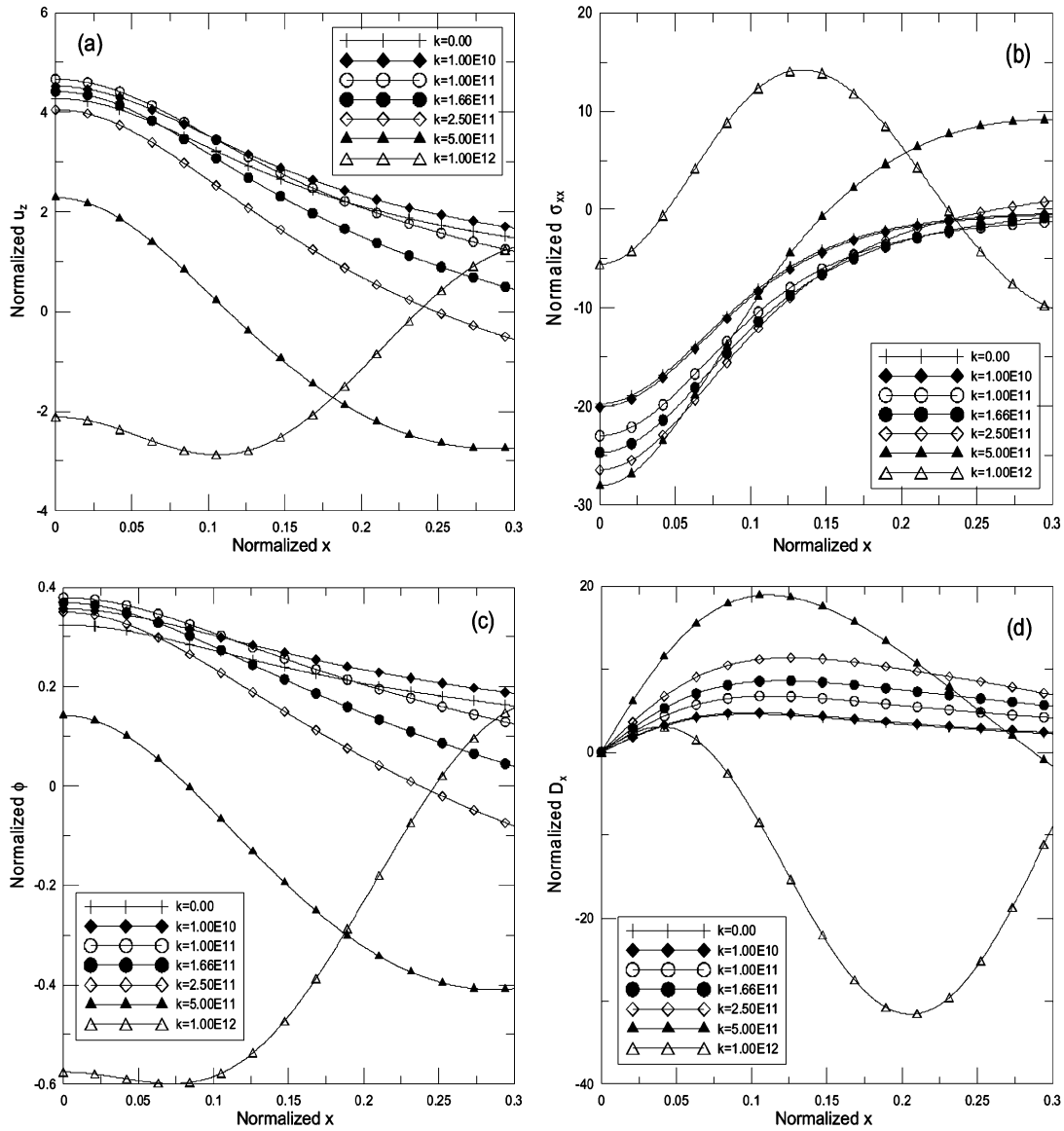
Figure 5. (a)–(d). Variation of field quantities along the surface line (from (0,0,0) to (0·3m,0,0)) of layered P/B/P half space (Model III), due to a point force at (0, 0, 0·15m) in z-direction and under general boundary condition with different spring constant k (in N/m^3). Displacement component u_z in (a), stress component σ_{xx} in (b), electric potential ϕ in (c), and electric displacement D_x in (d).

7. Conclusions

In this paper, the 3D Green's functions for transversely isotropic piezoelectric and multilayered half-spaces have been derived. Two systems of vector functions and the propagator matrix method are employed to obtain the Green's function solutions in a concise and unified form. Since the physical-domain Green's functions involve improper integrals of Bessel functions, the adaptive Gauss quadrature approach is applied to accelerate the convergence of the numerical integral. The solutions are for the general boundary condition along the surface of

the layered half-space, and thus include the spring-like case as well as the homogeneous case where the extended displacements and tractions are separated in the boundary-condition equations. Numerical examples are presented for four different half-space models and the effect of material stacking sequence and anisotropy are clearly illustrated. The effect of the spring constant in the spring-like boundary conditions has also been studied. This shows that, when the spring constant is relatively large, the response curve can be completely different to that when it is small or when it is equal to zero, with the latter being the traction-free insulating homogeneous boundary condition case. While the numerical results may have applications in different areas where layered structures are involved, the methodology may also be extended to 2D and 3D problems involving other concentrated sources, such as eigenstrain and dislocation.

Appendix A. Nonzero elements of coefficient matrix [*A*] in Equation (20)

$$A_{12} = \lambda^2(\varepsilon_{33}C_{13} + e_{33}e_{31})/\Delta \; ; \; A_{13} = \varepsilon_{33}/\Delta \; ; \; A_{16} = e_{33}/\Delta,$$
$$A_{21} = -1 \; ; \; A_{24} = 1/C_{44} \; ; \; A_{25} = -e_{15}/C_{44} \; ; \; A_{34} = \lambda^2,$$
$$A_{42} = \lambda^2\{C_{11} - [C_{13}(\varepsilon_{33}C_{13} + e_{33}e_{31}) + e_{31}(e_{33}C_{13} - C_{33}e_{31})]/\Delta \},$$
$$A_{43} = -(\varepsilon_{33}C_{13} + e_{33}e_{31})/\Delta \; ; \; A_{46} = (e_{31}C_{33} - e_{33}C_{13})/\Delta,$$
$$A_{52} = \lambda^2(e_{33}C_{13} - C_{33}e_{31})/\Delta; \; A_{53} = e_{33}/\Delta; \; A_{56} = -C_{33}/\Delta,$$
$$A_{64} = \lambda^2 e_{15}/C_{44}; \; A_{65} = -\lambda^2(\varepsilon_{11} + e_{15}^2/C_{44}),$$

where $\Delta = e_{33}^2 + C_{33}\varepsilon_{33}$

Appendix B. Nonzero elements of coefficients matrix [*W*] in Equation (21)

$$W_{12} = (\varepsilon_{33}C_{13} + e_{33}e_{31})/\Delta \; ; \; W_{13} = \varepsilon_{33}/\Delta \; ; \; W_{16} = e_{33}/\Delta,$$
$$W_{21} = -1 \; ; \; W_{24} = 1/C_{44}; \; W_{25} = -e_{15}/C_{44}; \; W_{34} = 1,$$
$$W_{42} = C_{11} - [C_{13}(\varepsilon_{33}C_{13} + e_{33}e_{31}) + e_{31}(e_{33}C_{13} - C_{33}e_{31})]/\Delta,$$
$$W_{43} = -(\varepsilon_{33}C_{13} + e_{33}e_{31})/\Delta \; ; \; W_{46} = (e_{31}C_{33} - e_{33}C_{13})/\Delta,$$
$$W_{52} = (e_{33}C_{13} - C_{33}e_{31})/\Delta; \; W_{53} = e_{33}/\Delta; \; W_{56} = -C_{33}/\Delta,$$
$$W_{64} = e_{15}/C_{44} \; ; \; W_{65} = -(\varepsilon_{11} + e_{15}^2/C_{44}),$$

where $\Delta = e_{33}^2 + C_{33}\varepsilon_{33}$

Appendix C. Material properties of PZT-4 and BaTiO$_3$

For the PZT-4, the elastic, piezoelectric, and dielectric coefficient matrices are respectively

$$[C] = \begin{bmatrix} 1\cdot39 & 0\cdot778 & 0\cdot743 & 0 & 0 & 0 \\ 0\cdot778 & 1\cdot39 & 0\cdot743 & 0 & 0 & 0 \\ 0\cdot743 & 0\cdot743 & 1\cdot15 & 0 & 0 & 0 \\ 0 & 0 & 0 & 0\cdot256 & 0 & 0 \\ 0 & 0 & 0 & 0 & 0\cdot256 & 0 \\ 0 & 0 & 0 & 0 & 0 & 0\cdot306 \end{bmatrix} (10^{11}\text{N/m}^2)$$

$$[e] = \begin{bmatrix} 0 & 0 & 0 & 0 & 12\cdot7 & 0 \\ 0 & 0 & 0 & 12\cdot7 & 0 & 0 \\ -5\cdot2 & -5\cdot2 & 15\cdot1 & 0 & 0 & 0 \end{bmatrix} (\text{C/m}^2)$$

$$[\varepsilon] = \begin{bmatrix} 0.64605 & 0 & 0 \\ 0 & 0.64605 & 0 \\ 0 & 0 & 0.561975 \end{bmatrix} (10^{-8}\text{CV}^{-1}\text{m}^{-1})$$

and for BaTiO$_3$ they are

$$[C] = \begin{bmatrix} 1.66 & 0.77 & 0.78 & 0 & 0 & 0 \\ 0.77 & 1.66 & 0.78 & 0 & 0 & 0 \\ 0.78 & 0.78 & 1.62 & 0 & 0 & 0 \\ 0 & 0 & 0 & 0.43 & 0 & 0 \\ 0 & 0 & 0 & 0 & 0.43 & 0 \\ 0 & 0 & 0 & 0 & 0 & 0.445 \end{bmatrix} (10^{11}\text{N/m}^2)$$

$$[e] = \begin{bmatrix} 0 & 0 & 0 & 0 & 11.6 & 0 \\ 0 & 0 & 0 & 11.6 & 0 & 0 \\ -4.4 & -4.4 & 18.6 & 0 & 0 & 0 \end{bmatrix} (\text{C/m}^2)$$

$$[\varepsilon] = \begin{bmatrix} 1.12 & 0 & 0 \\ 0 & 1.12 & 0 \\ 0 & 0 & 1.26 \end{bmatrix} (10^{-8}\text{CV}^{-1}\text{m}^{-1})$$

8. Acknowledgement

References

1. Y.A. Melnikov, *Green's Functions in Applied Mechanics.* Southampton-Boston: Computational Mechanics Publications (1995) 277 pp.
2. Y.A. Melnikov, *Influence Functions and Matrices.* New York-Besel: Marcel Dekker (1998) 488 pp.
3. T.C.T. Ting, *Anisotropic Elasticity*. Oxford: Oxford University Press (1996) 570pp.
4. E. Pan, Three-dimensional Green's functions in anisotropic half space with general boundary conditions. *J. Appl. Mech.* 70 (2003) 101–110.
5. E. Pan, Static Green's functions in multilayered half spaces. *Appl. Math. Modelling* 21 (1997) 509–521.
6. J.J. Liao and C.D. Wang, Elastic solutions for a transversely isotropic half-space subjected to a point load. *Int. J. Rock Mech. Min. Sci.* 6 (1998) 425–447.
7. Z.Q. Yue and H.T. Xiao, Generalized Kelvin solution based boundary element method for crack problems in multilayered solids. *Eng. Anal. Bound. Elem.* 26 (2002) 691–705.
8. C.D. Wang and J.J. Liao, Elastic solutions for a transversely isotropic half-space subjected to buried asymmetric-loads. *Int. J. Numer. Anal. Meth. Geomech.* 23 (1999) 115–139.
9. B. Yang and E. Pan, Efficient evaluation of three-dimensional Green's function in anisotropic elastostatic multilayered composite. *Eng. Anal. Bound. Elem.* 26 (2002) 355–366.
10. C.D. Wang, C.S. Tzeng, E. Pan and J.J. Liao, Displacements and stresses due to a vertical point load in an inhomogeneous transversely isotropic half-space. *Int. J. Rock Mech. Min. Sci.* 40 (2003) 667–685.

11. M.L. Dunn and H.A. Wienecke, Half-space Green's functions for transversely isotropic piezoelectric solids. *J. Appl. Mech.* 66 (1999) 675–679.
12. H.J. Ding, B. Chen and J. Liang, On the Green's functions for two-phase transversely isotropic piezoelectric media. *Int. J. Solids Struct.* 34 (1997) 3041–3057.
13. W.Q. Chen, T. Shioya and H.J. Ding, The elasto-electric field for a rigid conical punch on a transversely isotropic piezoelectric half-space. *J. Appl. Mech.* 66 (1999) 764–771.
14. E. Pan and F. Tonon, Three-dimensional Green's functions in anisotropic piezoelectric solids. *Int. J. Solids Struct.* 37 (2000) 943–958.
15. E. Pan, Mindlin's problem for an anisotropic piezoelectric half space with general boundary conditions. *Proc. R. Soc. London A* 458 (2002) 181–208.
16. E. Pan and F.G. Yuan, Three-dimensional Green's functions in anisotropic piezoelectric bimaterials. *Int. J. Eng. Sci.* 38 (2000) 1939–1960.
17. E. Pan, Some new three-dimensional Green's functions in anisotropic piezoelectric bimaterials. *Electr. J. Bound. Elements* 1 (2003) 236–269.
18. E. Pan, Three-dimensional fundamental solutions in multilayered piezoelectric solids. *Chinese J. Mech. Ser. A* 19 (2003) 127–132.
19. E. Pan, Static response of a transversely isotropic and layered half-space to general surface loads. *Phys. Earth Planet. Inter.* 54 (1989) 353–363.
20. E. Pan, Static response of a transversely isotropic and layered half-space to general dislocation sources. *Phys. Earth Planet. Inter.* 58 (1989) 103–117.
21. F. Gilbert and G. Backus, Propagator matrices in elastic wave and vibration problems. *Geophysics* 31 (1966) 326–332.
22. Z.Y. Ding and Y.Q. Shen, Quasi-static response of a layered viscoelastic half-space to general surface loading. *Phys. Earth Planet. Inter.* 66 (1991) 278–289.
23. J. Huang, The general model of static responses in multilayered elastic media. *Crust. Deform. Earthquake* 11 (1991) 1–6.
24. E. Pan, Exact solution for simply supported and multilayered magneto-electro-elastic plates. *J. Appl. Mech.* 68 (2001) 608–618.
25. E. Pan and P. Heyliger, Free vibrations of simply supported and multilayered magneto-electro-elastic plates, *J. Sound Vib.* 253 (2002) 429–443.
26. A.D. Chave, Numerical integration of related Hankel transforms by quadrature and continued fraction expansion. *Geophysics* 48 (1983) 1671–1686.
27. S.K. Lucas, Evaluating infinite integrals involving products of Bessel functions of arbitrary order. *J. Comput. Appl. Math.* 64 (1995) 269–282.
28. E. Pan, Green's functions in layered poroelastic half-spaces. *Int. J. Numer. Anal. Meth. Geomech.* 23 (1999) 1631–1653.
29. X. Wang and Z. Zhong, Three-dimensional solution of smart laminated anisotropic circular cylindrical shells with imperfect bonding. *Int. J. Solids Struct.* 40 (2003) 5901–5921.